Bridging Three Orders of Magnitude: Multiple Scattered Waves Sense Fractal Microscopic Structures via Dispersion

Simon A. Lambert,[1,2,*] Sven Peter Näsholm,[3] David Nordsletten,[2] Christian Michler,[2] Lauriane Juge,[4,5] Jean-Michel Serfaty,[6] Lynne Bilston,[4,7] Bojan Guzina,[8] Sverre Holm,[9] and Ralph Sinkus[2]

[1]*Centre de Recherche sur l'Inflammation (CRI), UMR 1149 Inserm—Université Paris Diderot, Paris 7, France*
[2]*King's College London, BHF Centre of Excellence, Division of Imaging Sciences and Biomedical Engineering, St. Thomas' Hospital, London SE1 7EH, United Kingdom*
[3]*NORSAR, P.O. Box 53, N-2027, Kjeller, Norway*
[4]*Neuroscience Research Australia, Randwick, Sydney, NSW 2031, Australia*
[5]*School of Medical Sciences, University of New South Wales, Sydney, NSW 2052, Australia*
[6]*CHU Xavier Bichat, Université Paris Diderot, APHP, U698 INSERM, CEFI, Paris 7, France*
[7]*Prince of Wales Clinical School, University of New South Wales, Sydney, NSW 2052, Australia*
[8]*Department of Civil, Environmental & Geo-Engineering, University of Minnesota, Minneapolis, Minnesota 55455, USA*
[9]*Department of Informatics, University of Oslo, P.O. Box 1080 Blindern, N-0316 Oslo, Norway*

(Received 29 December 2014; revised manuscript received 17 March 2015; published 26 August 2015)

Wave scattering provides profound insight into the structure of matter. Typically, the ability to sense microstructure is determined by the ratio of scatterer size to probing wavelength. Here, we address the question of whether macroscopic waves can report back the presence and distribution of microscopic scatterers despite several orders of magnitude difference in scale between wavelength and scatterer size. In our analysis, monosized hard scatterers 5 μm in radius are immersed in lossless gelatin phantoms to investigate the effect of multiple reflections on the propagation of shear waves with millimeter wavelength. Steady-state monochromatic waves are imaged *in situ* via magnetic resonance imaging, enabling quantification of the phase velocity at a voxel size big enough to contain thousands of individual scatterers, but small enough to resolve the wavelength. We show in theory, experiments, and simulations that the resulting coherent superposition of multiple reflections gives rise to power-law dispersion at the macroscopic scale if the scatterer distribution exhibits apparent fractality over an effective length scale that is comparable to the probing wavelength. Since apparent fractality is naturally present in any random medium, microstructure can thereby leave its fingerprint on the macroscopically quantifiable power-law exponent. Our results are generic to wave phenomena and carry great potential for sensing microstructure that exhibits intrinsic fractality, such as, for instance, vasculature.

DOI: 10.1103/PhysRevLett.115.094301 PACS numbers: 46.40.Cd, 46.80.+j, 83.85.Fg, 89.75.-k

Introduction.—Wave scattering has been shown to provide profound insight into the structure and dynamics of matter in the context of light [1–3], acoustics [4,5], geophysics [6], and particle scattering [7]. Various models of wave propagation have been developed in disordered media to describe the interaction between waves and scatterers present in the medium. Thereby, the underlying microstructure can be related to macroscopically observable wave characteristics. In the case of weakly fluctuating random media and thin sample dimensions, it is typically assumed that the wave interacts only once with the scatterers, leading to the Born approximation. In optics, this approach has been used to characterize the underlying spatial fractality in the refractive index of thin tissue samples [1]. As the number of scattering events increases, the single scattering approximation becomes invalid and higher orders of the Born expansion have to be used to take multiple scattering into account [8].

Recent advances in magnetic resonance imaging enable the direct visualization of monochromatic steady-state elastic waves in 3D [9]. Thereby, wave propagation processes and in particular multiple scattering effects in complex media can be observed *in situ* at subwavelength image resolution. This allows pixelwise quantification of phase velocity and dispersion properties [10]. Here, we try to answer the following fundamental question: Do the dispersion characteristics of multiple scattered waves allow us to uncover the presence and distribution properties of microscopic scatterers despite several orders of magnitude difference in scale between the wavelength and scatterer size? Thus, we are investigating the situation where the wavelength λ ($\sim$3 mm) is much larger than the average geometrical distance between scatterers ($\sim$30 μm)—hence, multiple scattering is taking place—and phase correlations do not vanish as the transport length l^* is much larger than the sample size [11]. This condition is characteristic for shear-wave to shear-wave scattering in the Rayleigh regime as the differential cross section is forward/backward and sideways collimated [12] and the scattering mean free path $l = (n\sigma)^{-1}$ is large ($\sim 10^4$ m) due to a small total

 © 2015 American Physical Society

shear-wave cross section $\sigma_s = (\pi a^2)(k_s a)^4$, with k_s the shear-wave vector, a the scatterer radius, and n the number density [13]. This precludes also any localization effects as $k_s l \gg 1$. Finally, imaging is done at spatial scales δ that allow local quantification of wave properties, but data acquisition cannot resolve spatially or temporally individual scattering events, i.e., $l^* > l \gg \lambda > \delta \gg a$.

The quest for extracting microstructural information from multiple scattering events is not new. In the field of geophysics, for instance, approaches such as "virtual source imaging" and "passive imaging" have been successfully developed for extracting the Green's function [14–16]. Here, imaging is made possible by the stochastic self-focusing of multiple scattered waves by subwavelength scatterers, which is the point in common with the present study. However, those methods utilize broadband signals that are not provided given our experimental situation.

The large difference between wavelength and scatterer radius, the small cross section, and the collimated forward/backward scattering of shear-wave to shear-waves places our problem in the domain of the O'Doherty-Anstey (ODA) theory [6]. This theory explains the transmission properties of a wavelet through a medium of finely stratified layers in 1D [17–19]. In the ODA theory, the superposition of multiple reflections leads to a propagating wavelet that consists of coherently superimposed multiple scattering events. While multiple scattering effects have already been studied successfully with ultrasound, those studies were done with wavelengths of a similar order as the scatterer radius ($\lambda/a = 0.47/0.4$ mm) [20,21]. The novelty of our analysis lies in the fact that we utilize the *in situ* dispersion properties of the shear-wave speed.

Theory of wave propagation in a multiple reflecting medium.—The ODA theory is valid under the assumption of small reflection coefficients and that space and time are interchangeable, i.e., a constant wave speed for the background material. The ODA model is rooted in the characterization of the scatterer distribution via its autocorrelation function, typically denoted as the "lag-time distribution" $p(t)$ describing the spatiotemporal distribution of scatterers. The lag-time distribution amounts to counting the number of occurrences of a given clearing distance between scatterers. The main result of the ODA theory is that the final transmitted pulse spectrum is expressed by $T(\omega) \propto e^{M(\omega)}$, where $M(\omega)$ is the one-sided discrete Fourier transform of the lag-time distribution. Here, we will use its continuous formulation as presented in Ref. [17]. Unlike typical ODA analyses that are mainly interested in the effect of beam attenuation, we consider here explicitly the propagative part of the ODA theory. The experimental data yield for each voxel the phase velocity c_p, which is related to the real part β of the complex wave vector $k = \beta - i\alpha$ via $\beta = \omega/c_p$. We can thereby relate the macroscopically observable propagative part β of the wave to the resulting microscopic phase change calculated via the ODA theory through

$$\begin{aligned} e^{-ikx} \propto e^{M(\omega)} &= e^{F(p(t))} \\ &\Rightarrow \beta \propto \frac{1}{x}\int_0^\infty p(r)\sin\left(\frac{r}{x}\right)dr \\ &\propto \omega \int_0^\infty p(t)\sin(\omega t)dt \end{aligned} \tag{1}$$

if we set the travel distance x to be a fraction of the wavelength within the lossless background material (F stands for the Fourier transform).

Medium characterization via lag-time distribution.—The lag-time distribution can be derived in general from the pair-correlation function $p(r)$ studied by Teixeira [7]. It counts the number of occurrences of a given clearing distance between scatterers. As shown by Hamburger *et al.* [22], any random distribution of particles exhibits sampling fluctuations at short distances below a characteristic length ζ_f. Therefore, the particle distribution $N(r)$ shows apparent fractality below ζ_f, i.e., $N(r) \propto r^{d_f}$, and Euclidean behavior above ζ_f, i.e., $N(r) \propto r^D$. Here, d_f stands for an apparent fractal dimension of the medium and D is the integer spatial dimension [see Fig. 1(a)]. The combination of the concepts from Teixeira and Hamburger *et al.* leads to a pair-correlation function $p(r) \propto r^{d_f - D}$ in the fractal domain and to a constant probability in the Euclidean region ($d_f = D$). The definition of the scatterer statistics has been studied in detail in Ref. [23]. Effectively, we are facing two cutoff values: a lower cutoff defined by the scatterer radius (representing a lag time of length zero) and an upper cutoff defined by ζ_f. The limited distance between those cutoffs in our case does not allow defining a rigorous fractal dimension, but rather an effective dimension to characterize the presence of non-Euclidean statistics. ζ_f evolves with density according to a pure geometric argument, namely $\zeta_f \propto \rho^{-1/D}$, and scales linearly with scatterer radius a for a constant density; i.e., overall we find $\zeta_f \propto a\rho^{-1/D}$ (neglecting the finite bead radius) [22].

The effect of the upper physical cutoff is handled via the introduction of exponential weighting functions [7]. Thus, the lag-time distribution p_{tot} is expressed as a sum of two contributions: a fractal-like component that decays exponentially with t/τ_f, and a nonfractal component that rises exponentially with t/τ_f ($\tau_f = \zeta_f/c_0$, where c_0 is the wave speed in the background material). The nonfractal component is eventually suppressed with the aid of the parameter $\tau_c \gg \tau_f$ to avoid infinitely long lag times that are not physical [7]. The presence of those cutoffs leads ultimately to the presence or absence of scattering induced dispersion depending on the ratio of the wavelength to ζ_f.

Figure 1(b) confirms the validity of this approach using 2D simulations of randomly distributed particles with

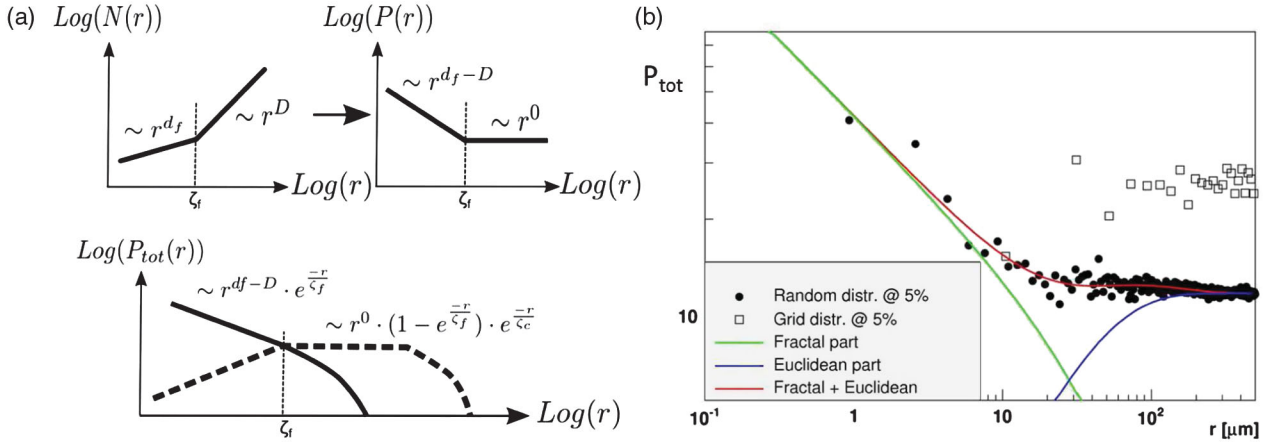

FIG. 1 (color). Characterization of lag-time distribution (2). (a) From particle to lag-time distribution and (b) verification via simulation.

radius $a = 5$ μm at low density $\rho = 5\%$. We will therefore define

$$p_{\mathrm{tot}}(t) = t^{d_f - D} e^{-(t/\tau_f)} + t^0 (1 - e^{-(t/\tau_f)}) e^{-(t/\tau_c)}. \quad (2)$$

Multiple reflections induce power-law dispersion in fractal-like media.—Equation (1) in combination with Eq. (2) leads to a description of wave propagation for the multiple scattered part of the beam by using Eqs. 3.944-5 and 3.893-1 from Ref. [24]

$$\beta^{\mathrm{scattered}} \propto \omega \tau_f^{df-D+1} \Gamma(d_f - D + 1)\,[1 + (\omega\tau_f)^2]^{[(D-d_f-1)/2]} \times \sin((df - D + 1)\tan^{-1}(\omega\tau_f)) + \frac{\omega\tau_c^2}{1 + (\omega\tau_c)^2} - \frac{\omega\tau_M^2}{1 + (\omega\tau_M)^2}, \quad (3)$$

where $\tau_M = [(\tau_c\tau_f)/(\tau_c + \tau_f)] \cong \tau_f$. When operating at sufficiently high frequencies such that $\omega\tau_f \gg 1$, we obtain

$$\beta^{\mathrm{scattered}} \propto \Gamma(d_f - D + 1)\ \omega^{D-d_f} \sin\left(\frac{\pi}{2}(df - D + 1)\right). \quad (4)$$

Overall, the total propagation is modeled as a weighted sum of the direct beam and the scattered beam, i.e.,

$$\beta^{\mathrm{total}} = \varepsilon\omega + \beta^{\mathrm{scattered}} \quad (5)$$

with unknown weight ε. This result demonstrates two things: the presence or absence of dispersion depending on whether the scatterer distribution is fractal-like (i.e., $d_f \neq D$) or Euclidean (i.e., $d_f = D$), and that the frequency dependence of the dispersion is governed by a power law [normalization factors have been omitted in Eqs. (3) and (4)].

The high frequency approximation of Eq. (4) probes solely the fractal-like contribution since the wavelength is sufficiently small compared to ζ_f. At the other end of the spectrum, where the wavelength is much larger than the characteristic length of the fractal region (i.e., $\omega\tau_f \ll 1$, but still $\omega\tau_c \gg 1$), one does not find any anomalous frequency dependence for the reflected part as the first term in Eq. (3) approaches zero. The remaining quadratic dependence on $(\omega\tau_M)^2$ is negligible compared to the direct beam, which propagates according to $\beta \propto \omega$. Hence, in that case the frequency dependence is governed by the direct beam and we formally return to a frequency-independent phase velocity because $c_p(\omega) = \omega/\beta(\omega) = \mathrm{const}$. The original ODA theory utilizes the properties of the lag-time distribution at $t = 0$ for estimating ε [Eq. (5)]. Here, that approach is not feasible due to a singular behavior of $p_{\mathrm{tot}}(t)$ for $t \to 0$ and ε must therefore be determined from a fit to the data.

Comparison between the predictions of Eq. (5) and experiments requires the following additional theoretical considerations.

(1) The ODA theory has been developed in 1D. Here, scattering can occur only in one direction. A 3D volume—characterized by its radius ζ_f—represents a domain providing more possibilities for scattering than a 1D structure with a length equal to $2\zeta_f$. It is therefore necessary to scale the results found for the correlation length ζ_f in 2D or 3D to an equivalent effective length in 1D for the ODA theory. Here, we follow a heuristic approach which is motivated by geometry: we determine the number of *equivalent* 1D models that fit into the area or volume delimited by $\zeta_f^{2D/3D}$. Intrinsically, a 1D model has no area or volume. We therefore use the bead size a as the only scale available and attribute to the 1D model the apparent area $(2\zeta_f^{2D})(2a)$

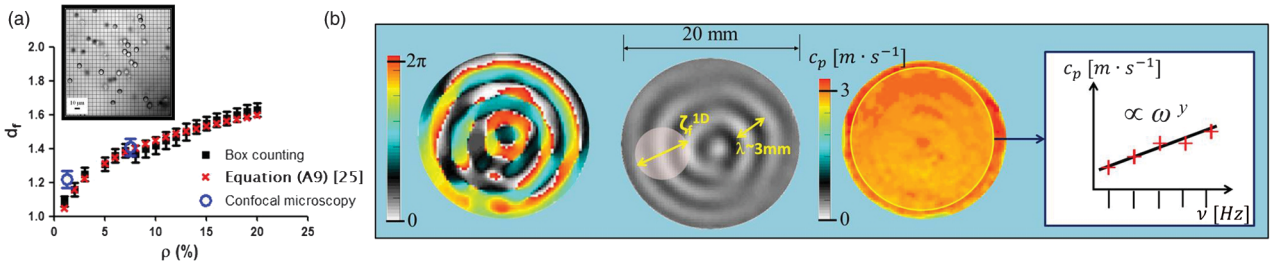

FIG. 2 (color). Characterization of gel samples and concept of shear-wave dispersion experiment. (a). Density dependence of fractal dimension. The inset shows a confocal microscopy image of a gel sample. (b) Phase of the main shear-wave displacement component and corresponding displacement in the through-slice direction as measured via MRE within a single slice of the gel sample. The wavelength λ (~3 mm) is comparable to the effective correlation length ζ_f^{1D} whereby apparent fractality can be probed. The third image shows the derived phase velocity c_p from which mean values of c_p are calculated (yellow circle). Note, that c_p is nearly constant as expected for a sample that appears homogeneous at the macroscopic imaging scale. Mean values of c_p acquired at different vibration frequencies represent the basis for the subsequent analysis exploring the exponent of the frequency power law (4th image).

for the 2D case. The ratio of these two areas, i.e. the area that is characterized by apparent fractal statistics $\pi(\zeta_f^{2D})^2$ and the apparent area $(2\zeta_f^{2D})(2a)$ represents the scale factor by which ζ_f^{2D} needs to be augmented to represent the corresponding effective length ζ_f^{1D}. Hence, we find $\zeta_f^{1D} = \zeta_f^{2D}[\pi(\zeta_f^{2D})^2/(2\zeta_f^{2D})(2a)] = \zeta_f^{2D}(\pi/4)(\zeta_f^{2D}/a) \propto a\rho^{-(2/D)}$. In our case we obtain $\zeta_f^{1D} \approx 8000\ \mu$m, which is comparable to wavelengths at the millimeter scale and can therefore be probed by our experiments.

(2) The apparent fractal dimension d_f evolves with the scatterer density [23]. Our theoretical prediction for $d_f(\rho)$ [25] is in very good agreement with results obtained from 2D simulations and from confocal microscopy images taken from the experimental scatterer samples, both analyzed with a box-counting method for fractal analysis [26] [see Fig. 2(a)].

(3) A power-law equation is fit to Eq. (5) according to $c_p = \omega/\beta^{\text{total}} \propto \omega^y$. This provides an effective apparent power-law exponent, where y is the exponent of the phase velocity [Fig. 2(b)].

Experiments.—The Magnetic Resonance Elastography (MRE) measurement technique leads inherently to an averaging process over several hundreds of wave oscillation periods. Thus, any temporal fluctuations of the field due to multiple scattering events are averaged out and only the mean field remains. The deviations from the mean field are principally the backscattered reflections, which have a zero temporal expectation value [17]. Extraction of the shear-wave phase velocity is explained in Ref. [10]. We use an agarose gel at a concentration that yields quasilossless behavior for shear waves over the investigated frequency range [27]. Apparent losses due to wave scattering are generated via the addition of colloidal suspensions of polystyrene microspheres with known radius ($a = 5\ \mu$m and $a = 15\ \mu$m) and concentrations (1%–20% volume fraction) prior to gel solidification [25]. The resulting shear modulus of the gel leads to a shear wavelength of about 3 mm for frequencies in the 600–1000 Hz range, yielding $\beta a \approx 0.01$.

Phase coherence can be observed throughout the entire sample, justifying the use of phase information for the ODA theory [Fig. 2(b)]. Individual scattering events are not resolvable as the average mean distance between scatterers is ~30 μm at a 5% microsphere density and an imaging resolution set to $300 \times 300 \times 400\ \mu\text{m}^3$. This particular pixel size was chosen to optimize on the one hand the sensitivity of the MRE method for providing reliable phase velocity data [28,29], and on the other hand to reach a statistical effect of the microsphere distribution at the scale of the voxel (540–10 800 spheres per voxel). Mean phase velocity values obtained from each sample are fit to a frequency power law.

Results.—Experimental data confirm that the gel is nondispersive in the absence of any microspheres, i.e., $y = 0$ [Fig. 3(a)]. The addition of microspheres at various concentrations leads to changes in the magnitude for c_p of not more than ~25% and to an increase of the slope y; i.e., the material become dispersive. Figure 3(b) shows the evolution of y with microsphere density: starting at zero for $\rho = 0$, it reaches a maximum at densities of around 7% and returns back to zero with a further increase of the scatterer density. This is expected for large densities due to a shrinking characteristic length scale ζ_f and an effective fractal dimension that approaches the upper limit, i.e., $d_f \to D$. The theoretical model stemming from Eq. (3) describes this evolution closely. The fit to the data yields a ratio between the scattered beam and the direct beam of about 10, which demonstrates that multiple scattering dominates. According to the theory, a further increase in the scatterer radius to $a = 15\ \mu$m does not change the dispersion properties, as experimentally confirmed for $\rho = 5\%$. Additional experiments were performed using polysaccharides as scatterers with an average diameter distribution of $2.3 \pm 1.4\ \mu$m. Experimental data confirm the expected reduction in the apparent dispersion and lie

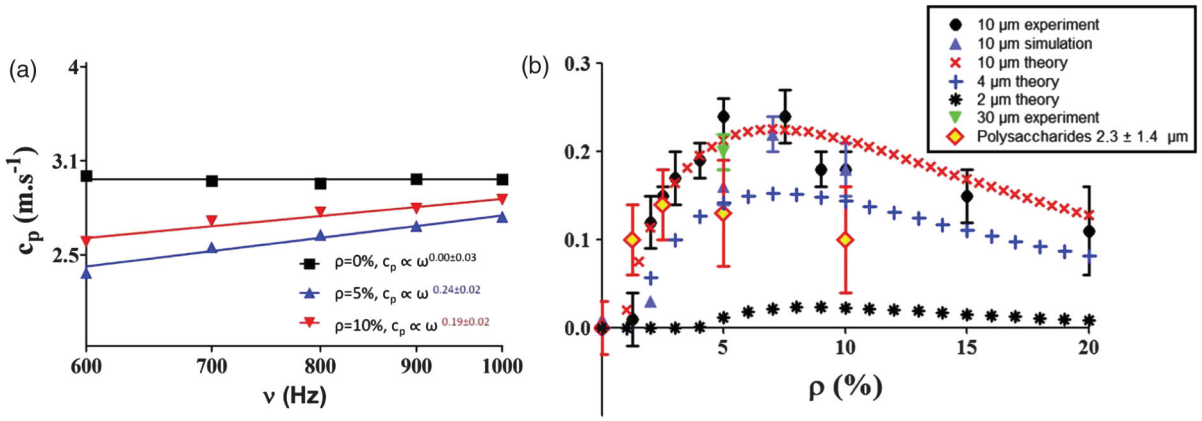

FIG. 3 (color). Geometrically induced dispersion due to fractal structures. (a) Frequency dependence of the phase velocity for various scatterer densities. (b) Density dependence of the power law exponent y for the experiment, simulation, and theory. Experimental data for scatterers of different diameters are in good agreement with our theory. Error bars are only shown when errors are larger than 1%.

approximately between the theoretical predictions for a 2 and 4 μm bead diameter. Additionally, finite element simulations using the classical viscoelastic wave equation were performed. Good agreement between the simulations, experiment, and theory was found. Simulations could not be extended beyond a 10% density due to convergence issues for the finite element solver.

Discussion and conclusions.—To infer microstructural heterogeneity from macroscopic dispersion, it is vital to construct a concrete underlying theory. In our work, we derive the presence of a dispersion power law from two conditions: first, apparent fractality of the scatterer distribution below an effective length that is of the order of the wavelength, and second, the presence of multiple reflections. Contrary to previous approaches, here we do not try to solve a simplified transport equation, but rather relate directly the geometrical details of the scatterer distribution to the propagation coefficient via its autocorrelation function. Our results demonstrate that the presence and characteristics of monosized scatterers can be revealed via the dispersion properties of the phase velocity at the macroscopic scale despite the minute ratio of the scatterer size to the wavelength, namely, $\beta a \in [0.007–0.012]$. In fact, the ability of waves to probe microstructure in our context is therefore determined by the ratio of the effective correlation length ζ_f^{1D} to the wavelength λ, which is here above unity with $\beta\zeta_f^{1D} \in [9–15]$. This provides enhanced sensitivity of the imaging method beyond its normal spatial resolution with the limiting factor being the spatial extent of the apparent fractality, not the size of the individual scatterers.

These findings are generic to wave propagation and show consistency with other reported wave phenomena. Recently, the case of light propagation in a fractal medium was studied by Barthelemy *et al.* [3]. Their experimental conditions fall into the regime $\omega\tau_f \gg 1$, i.e., Eq. (4) applies. Anomalous propagation properties were observed as long as $d_f \neq D$. Light diffusion returned to classical statistics for the case of a densely packed material with monosized spheres. This situation corresponds to a Euclidian lag-time distribution [$d_f = D$; Fig. 1(b), open squares] and hence to the absence of anomalous effects, in agreement with Eq. (4).

More complex structures will lead to effective fractal dimensions that depend not only on density, but also on other structural characteristics. This has great potential in medical applications. Hypothesizing that the contrast ratio between the microvasculature and the background tissue is strong enough, the characterization of the organization of vascularized tissues via shear waves would provide a novel mechanism for assessing vascular changes.

We thank Jose Teixeira and Marianne Lambert for helpful discussions about the theory developed here. We thank also Samira Benadda for her assistance with the confocal microscope of the "Plateau d'Imagerie Cellulaire et tissulaire de l'Institut Claude Bernard-IFR2-INSERM". We are also grateful to people from "plateforme CEFI" for their leading role in creating the 7T facility. We thank Cédric Chauvière for the fabrication of polysaccharides. We also thank Prof. Xing Cai, Simula Research Laboratory, Oslo, Norway for help with initial simulations. This research was funded/supported by the National Institute for Health Research (NIHR) Biomedical Research Centre based at Guy's and St Thomas' NHS Foundation Trust and King's College London. The views expressed are those of the author(s) and not necessarily those of the NHS, the NIHR or the Department of Health. Part of this work was funded by the Institut National du Cancer (Project No. 2010-1-RT-03-INSERM 7-1). The work of SPN was done while at the Department of Informatics, University of Oslo and partly financed by the Norwegian Research Council. The research leading to these results has received

funding from the European Research Council under the European Union's Seventh Framework Programme (FP/2007-2013)/ERC Grants Agreement No. 600948 and No. 601055.

*Corresponding author.
simon.lambert@kcl.ac.uk; simonlambert2@gmail.com

[1] J. M. Schmitt and G. Kumar, Opt. Lett. **21**, 1310 (1996).
[2] M. Xu and R. R. Alfano, Opt. Lett. **30**, 3051 (2005).
[3] P. Barthelemy, J. Bertolotti, and D. S. Wiersma, Nature (London) **453**, 495 (2008).
[4] J. H. Page, P. Sheng, H. P. Schriemer, I. Jones, X. D. Jing, and D. A. Weitz, Science **271**, 634 (1996).
[5] A. Tourin, M. Fink, and A. Derode, Wave Random Media **10**, R31 (2000).
[6] R. F. O'Doherty and N. A. Anstey, Geophysical Prospecting **19**, 430 (1971).
[7] J. Teixeira, J Appl. Crystallogr. **21**, 781 (1988).
[8] L. Ryzhik, G. Papanicolaou, and J. B. Keller, Wave Motion **24**, 327 (1996).
[9] R. Muthupillai, D. J. Lomas, P. J. Rossman, J. F. Greenleaf, A. Manduca, and R. L. Ehman, Science **269**, 1854 (1995).
[10] R. Sinkus, K. Siegmann, T. Xydeas, M. Tanter, C. Claussen, and M. Fink, Magn. Reson. Med. **58**, 1135 (2007).
[11] M. Haney, K. v. Wijk, and R. Snieder, Geophysics **70**, T1 (2005).
[12] R. S. Wu, Pageoph **131**, 605 (1989).
[13] V. A. Korneev and L. R. Johnson, Pageoph **147**, 675 (1996).
[14] R. Snieder, Phys. Rev. E **69**, 046610 (2004).
[15] R. Snieder, J. Sheiman, and R. Calvert, Phys. Rev. E **73**, 066620 (2006).
[16] F. Mulargia and S. Castellaro, Phys. Rev. Lett. **100**, 218501 (2008).
[17] N. Banik, l. Lerche, and R. Shuey, Geophysics **50**, 2768 (1985).
[18] H. Sato, J. Acoust. Soc. Am. **71**, 559 (1982).
[19] L. Wennerberg and A. Frankel, Bull. Seismol. Soc. Am. **79**, 1287 (1989).
[20] A. Derode, A. Tourin, and M. Fink, Phys. Rev. E **64**, 036605 (2001).
[21] A. Derode, A. Tourin, and M. Fink, Phys. Rev. E **64**, 036606 (2001).
[22] D. Hamburger, O. Biham, and D. Avnir, Phys. Rev. E **53**, 3342 (1996).
[23] M. Ciccotti and F. Mulargia, Phys. Rev. E **65**, 037201 (2002).
[24] I. S. Gradshetyn and I. M. Ryzhik, *Table of Integrals, Series, and Products*, 7th ed. (Academic Press, Burlington, MA, 2007).
[25] See Supplemental Material at http://link.aps.org/supplemental/10.1103/PhysRevLett.115.094301 for additional information on the probability distribution, phantom fabrication, optical microscopy, and Magnetic Resonance Elastography setup.
[26] T. G. Smith, Jr., G. D. Lange, and W. B. Marks, J. Neurosci. Methods **69**, 123 (1996).
[27] Y. Yamakoshi, J. Sato, and T. Sato, IEEE Trans. Ultrason. Ferroelectr. Freq. Control **37**, 45 (1990).
[28] S. Papazoglou, U. Hamhaber, J. Braun, and I. Sack, Phys. Med. Biol. **53**, 3147 (2008).
[29] R. Sinkus, M. Tanter, T. Xydeas, S. Catheline, J. Bercoff, and M. Fink, Magn. Reson. Imaging **23**, 159 (2005).